

Techno-economic design and evaluation of autonomous micro-grid for a remote area in Sinai-Egypt: Ras-Shaitan case study

Dina Emad

Electrical Power and Machine
Department
Faculty of Engineering
Zagazig, Egypt
eng_dina.emad@yahoo.com

M.A. El-Hameed

Electrical Power and Machine
Department
Faculty of Engineering
Zagazig, Egypt
m_a_elhameed@yahoo.com

M.T.Yousef

Electrical Power and Machine
Department
Faculty of Engineering
Zagazig, Egypt

A.A. El-Fergany

Electrical Power and Machine
Department
Faculty of Engineering
Zagazig, Egypt
el_fergany@ieec.org

Abstract— This paper proposes a techno-economic design and evaluation of a stand-alone micro-grid. It comprises PV/wind/battery system to feed a remote area called Ras- Shaitan, in Sinai-Egypt. The meteorological data for the selected area regarding temperature, wind speed and sun irradiation are collected and analyzed. Necessary modeling and technical specifications of system components are decided along with the load profile. System design is based on minimizing the net present cost (NPC) while keeping technical constraints including the continuity of supply. Homer software is utilized to get the optimal and cost-effective components' size. System performance analysis including cost analysis and hourly energy balance are performed to evaluate the proposed design. Effect of varying the average daily load demand on system size and cost is presented. Finally, the effect of renewable resources fluctuations on system design and cost is also included.

Keywords— *Micro-grid; PV/wind/battery; Homer; net present cost; cost of energy;*

I. INTRODUCTION

Approximately 1.5 billion people had no electricity access, of which 95% were living in remote areas [1]. Electricity crisis around the world lies in its generation process. The majority of electricity production is got from fossil fuels, which cause environmental problems and expected to be exhausted in the following years. Increasing costs of fuel and its transportation is additional obstacle [2]. On the other hand, renewable energy (RE) technologies has minimal environmental problems and their cost is decreasing with time. Remote areas may be rich with RE resources (wind and sun). Therefore, RE would be a good choice for these areas to be supplied by electricity compared with grid extension or fossil fuel based generation [3]. The international energy agency [4] expected that RE sharing in global electricity mix will be increased to 30% in 2022, with 82% sharing of photovoltaics (PV) and wind turbines (WT). PV and WT are considered the most committed energy sources alternatives for remote areas, as they may complete each other.

At periods of poor solar radiation, wind speed may be found high and WT power could compensate the decrease in solar power production [5].

RE resources had various combinations, small loads could be supplied by PV-battery or wind-battery system, while higher load required PV-wind sources. Due to fluctuations in wind speeds and solar radiations, micro-grids would have a lack of flexibility and reliability. This problem is solved by integrating energy storage system (ESS), it stores excess RE energy and reuses it in periods of low energy generations [6]. Among these ESS, batteries are the most used tool for energy storage [7]. Till now, other alternatives such as fuel cells and hydrogen tanks have higher cost and low efficiency of conversion from electricity to hydrogen and from hydrogen back to electricity [8].

RE modeling, simulation, and sizing has attracted many researches to reach the most economic system components [3, 9-15]. Due to the fluctuating nature of solar radiation, wind speed and the incompatibility between load and RE power generated, the designed system may suffers from load loss and/or high capital cost. In order to handle this problem, classical, meta-heuristic techniques and computer programs are applied for optimal system design. The objective function in some studies depends mainly on cost of energy (COE) minimization [16, 17], while in other studies it includes the loss of power supply probability as well [18].

Computer programs for micro-grids design were reviewed in [19]. Among them, Homer (Hybrid optimization model for electrical renewable) is the most used package for stand-alone systems [20-24]. Homer simulates and analyzes systems for optimal sizes based on meteorological and load data of the area under study. Homer has been used in [20] to get the optimal PV\WT\battery system size based on net present cost (NPC), the system supplies electricity to a remote island. Another hybrid system combination of hydro-power, bio-diesel generator, PV and WT was optimally designed using Homer [22]. Results obtained for a stand-alone system are compared with

conventional grid extension confirming the cost-effectiveness of the proposed system over grid extension choice. Homer is used in [23] for designing a hybrid PV, WT and hydrogen storage system. A study in Colombia was discussed in [24] to supply three villages with electricity. The sources of PV, wind and diesel generators were introduced to Homer to select the most economic combination based on NPC, initial cost (IC), or COE.

In this paper, a hybrid micro-grid comprising PV/WT/battery system is designed to supply electricity to a tourist area in Egypt. System design is based on minimizing NPC while keeping technical constraints including the continuity of supply. Effectiveness of the proposed system is proved by evaluating cost analysis and hourly energy balance. Moreover, average daily load demand is varied to study its effect on system size and cost. The effect of renewable resources fluctuations on system design and cost is also included.

The rest of paper is organized as follows; section 2 provides the area site information and its meteorological data. Section 3 describes the system configuration, components modeling and costs. In section 4, results and discussions are presented. The final concluded remarks are given in section 5.

II. SITE INFORMATION

In this study, a stand-alone micro-grid is designed to supply power to a remote area in Egypt, Sinai near Nuweiba city called Ras Shaitan (longitude: 34° 41', latitude: 29° 7'). A google earth snapshot of this area is illustrated in Fig. 1. This area is full of sunshine and wind, so it will be a good choice for design a stand-alone micro-grid to supply the load with electric power. The meteorological data for this area is obtained from the Nasa web site [25]. The average solar insolation is 5.65 kWh/m²/day, average wind speed is 4 m/s and average temperature is 19.52 °C for the 2018 year. The average monthly wind speed and solar insolation with a clearness index are shown in Fig. 2. The hourly solar irradiance with wind speed were highlighted as shown in Fig. 3 for three days from 27 to 29 Sept. These selected days show that in some periods complementary between solar irradiance and wind energy is found. Where, in cloudy days where solar irradiance is week, wind speed is high.

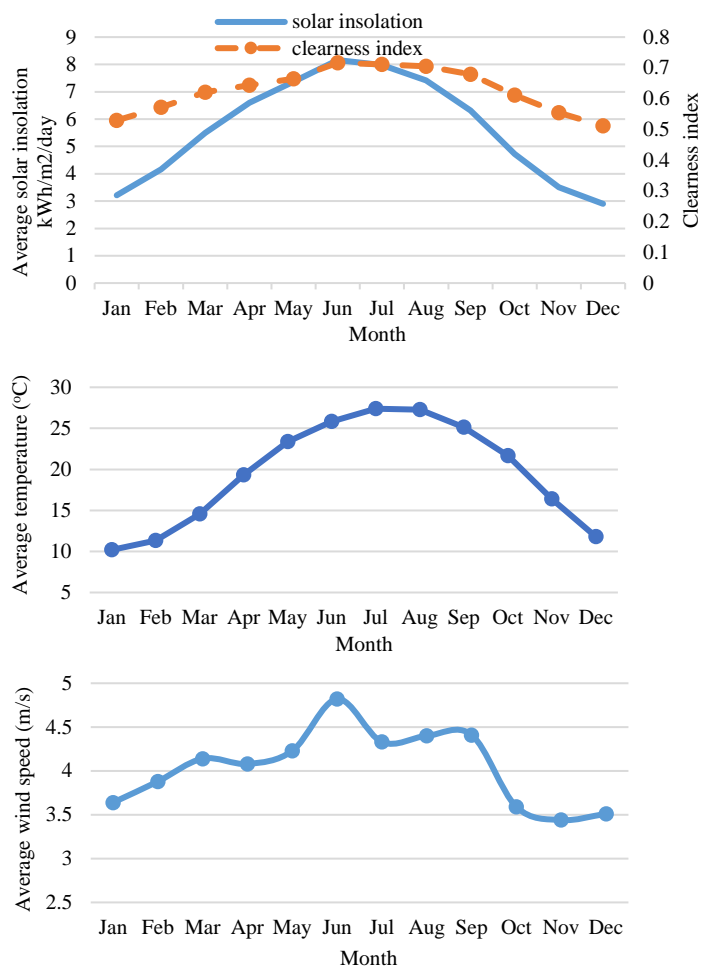


Fig.2 meteorological data (a) average solar radiation, (b) average temperature and (c) average wind speed.

III. MICRO-GRID CONFIGURATION

The micro-grid is composed of PV and WT as energy sources and battery banks as energy storage devices. In addition to inverters and other cables for distribution requirements.



Fig. 1 location of RAS-Shaitan on google earth

When the generated power from PV and WT is greater than demand power, the excess power is utilized to charge the battery banks until their maximum charge limit. If the battery bank is fully charged, excess power is dumped as the system is a stand-alone. When the generated power cannot cover the demand power, energy deficiency is then supplied from the battery banks. System configuration and flow of power are shown in Fig.4 . The battery bank is the only dispatchable source, hence the system can be easily controlled. Batteries charge or discharge is based on the power difference between RE sources and load, and the batteries state of charge (SOC).

A. Load profile

The daily base load is estimated as 357 kWh/day with 53 kW peak demand. The hourly load curve is derived by adding randomness. This is achieved by adding hourly and daily perturbation coefficients as given by (1) [26].

$$k_p = 1 + \phi_d + \phi_h \quad (1)$$

Where ϕ_d is the daily random variability factor which detects the variation day by day and ϕ_h is the step time random variability. In this study, the time step had been taken as one hour, then ϕ_h is the hourly variation percent.

Both the time step and day by day random variability factor are set to 20%. The produced load curve is shown in Fig. 5 .

B. PV system

The PV used is the Suntech Polycrystalline solar panel with rated power at of 265W standard test conditions (STC). Its efficiency under STC is 16.3%. Complete information is summarized in Table 1. Capital and replacement costs are extracted from [27], while operational and maintenance costs are neglected [20]. The output power of PV in W is given by (2) [28].

$$P_{pv} = P_{pvstc} \cdot F_{pv} \cdot \left(\frac{G(t)}{G_{stc}} \right) \cdot [1 + \alpha_p (T_c - T_{stc})] \quad (2)$$

$$T_c = T_{amb}(t) + \left(\frac{NOCT-20}{800} \right) * G(t) \quad (3)$$

Where P_{pvstc} is the rated capacity of PV array at STC (W), $G(t)$ is the instantaneous global solar radiation incident on PV array (W/m^2), F_{pv} is the PV derating factor due to dust, shadow and other weather conditions [29]. α_p is the temperature coefficient of PV array power, T_c is cell temperature ($^{\circ}C$) and T_{stc} is cell temperature at STC. $T_{amb}(t)$ is the ambient temperature. $NOCT$ is the normal operating cell temperature. G_{stc} is the solar radiation at STC. F_{pv} is assumed as 80% and α_p is $-0.41\%/^{\circ}C$ according to the solar panel's data sheet.

C. Wind turbine

The selected wind turbine is Foshan type. Its specifications are presented in Table 2. The power curve for the WT is shown in Fig. 6

In case of availability of power curve, the time step wind power is given by (4) [30]

$$P_{wt}(t) = P_{wtr} * \left[l_1 * e^{-\left(\frac{v(t)-d_1}{h_1} \right)^2} + l_2 * e^{-\left(\frac{v(t)-d_2}{h_2} \right)^2} + l_3 * e^{-\left(\frac{v(t)-d_3}{h_3} \right)^2} \right] \quad (4)$$

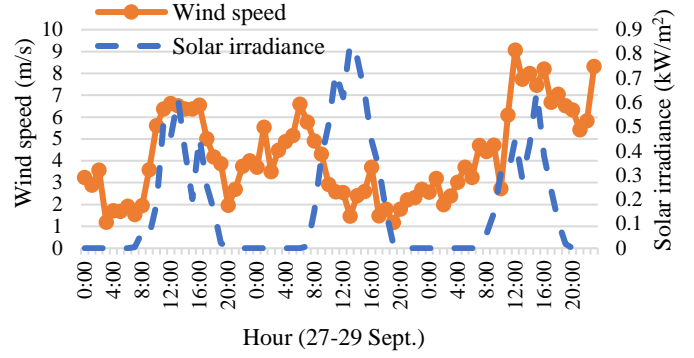


Fig. 3 hourly solar and wind resources for 3 days

Where $l_1, l_2, l_3, d_1, d_2, d_3, h_1, h_2$ and h_3 are the regression coefficients from power curve, P_{wtr} is the rated power (kW) and $v(t)$ is the wind speed at hub height. Each turbine has its own hub height. The measured wind speed can be recalculated at hub height due to a power law as given in (5).

$$v(t) = v_{anem}(t) * \left(\frac{H_{wt}}{H_{anem}} \right)^{\gamma} \quad (5)$$

Where $v_{anem}(t)$ is the wind speed at anemometer height (10 m in this study), H_{wt} and H_{anem} are the hub height and anemometer height and γ is the Hellmann exponent usually between 0.1 to .25 based on the nature of the studied zone (assumed 0.25).

D. Battery banks

The specifications of the Hoppecke battery bank used in this study are given in Table 3 . Equations to determine the number of required batteries are given by (6)-(8).

$$C_{Ah} = \frac{n_{day} * E_{load}}{\eta_{batt} * DOD * V_{batt} * \eta_{inv}} \quad (6)$$

$$n_{batt} = \frac{C_{Ah}}{C_{batt}} \quad (7)$$

$$n_{string} = \frac{n_{batt}}{(V_{bus}/V_{batt})} \quad (8)$$

Where n_{day} is the autonomy days powered by the battery; E_{load} is the energy required per day; η_{batt} is the battery efficiency; η_{inv} is the inverter efficiency; DOD is the maximum depth of discharge; V_{batt} is the nominal battery voltage; V_{bus} is the DC bus bar voltage; C_{batt} is the total ampere-hour (Ah) storage for single battery; C_{Ah} is the total storage capacity required in Ah; n_{string} is the number of battery strings.

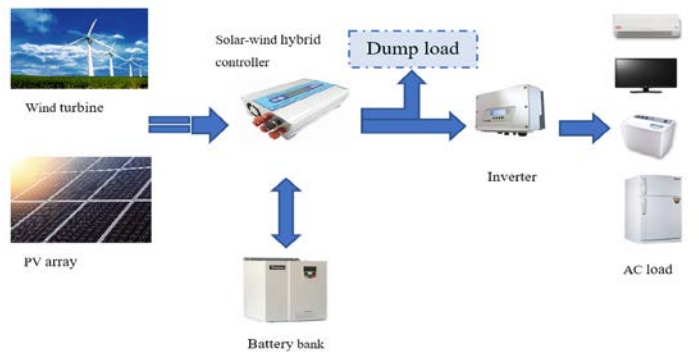


Fig.4 system configuration and power flow

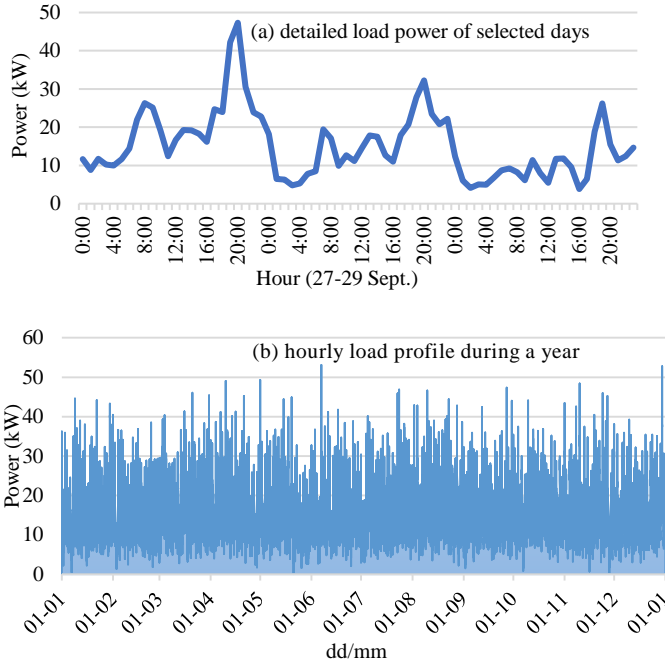


Fig. 5 AC Load profile and hourly data

The batteries kinetic model considered them as composed of two tanks [29, 31]. The first tank can supply the load with the available energy but the second is chemically controlled by charging and discharging rate. The SOC also controls the charging and discharging process of energy. When renewable energy is greater than load demand, the excess energy will charge the battery banks until its maximum SOC. On the other hand, when renewable energy cannot meet load demand, the battery banks will supply load to its minimum SOC.

From Battery data sheet, owing to cycles to failure curve and capacity curve Fig.7 (a)-(b), the lifetime throughput can be calculated related to the number of cycles to failure as given by (9).

Table 1 PV module details

Manufacture	Suntech solar panel	No. of cells	60 (6×10)
Model	Polycrystalline	Dimensions mm	1640×992×35
Max power at STC (P_{max})	265 W	Power tolerance	0/+5 W
Optimum operating voltage at STC (V_{mp})	31.0 V	Capital cost	450 \$/kW
Optimum operating current at STC (I_{mp})	8.56 A	Lifetime	25 years
Normal operating cell temperature (NOCT)	45±2 °C	Module efficiency	16.3%
Temperature coefficient of P_{max}	-0.41 %/°C		

Table 2 Wind turbine details

Manufacture	Foshan Ouyad Ltd.	Rated voltage	220/240 v
Rated Power	10 kW	Capital cost	5050 \$/unit
Max. power	10.2 kW	Replacement cost	5050 \$/unit
Cut-in wind speed	3.0 m/s	Operational and maintenance cost (O&M)	10 \$/unit/year
Rated wind speed	12 m/s	Hub height	15 m
Cut-out wind speed	25 m/s	Lifetime	20 years
Survival wind speed	60 m/s		

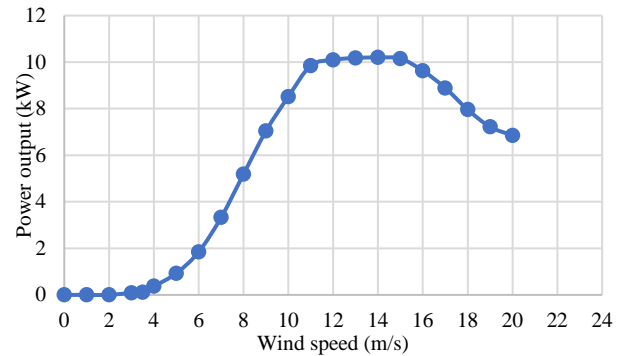


Fig. 6 Foshan wind turbine power curve

$$Q_{th} = n_f * d * \frac{C_{max} * V_{batt}}{1000} \quad (9)$$

Where Q_{th} is the kWh lifetime throughput of one battery; n_f is the number of cycles to failure; d is the depth of discharge (%); C_{max} is the battery maximum capacity (Ah).

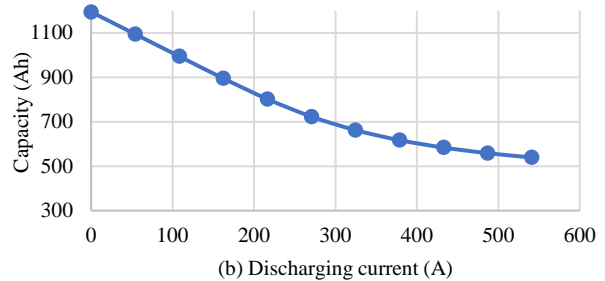
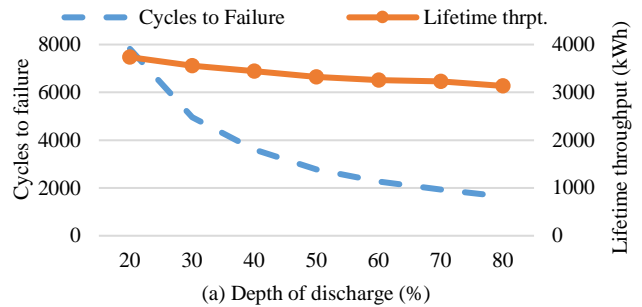


Fig.7 battery discharging characteristics

E. Converters

The generated power from PV is DC and that from the selected wind turbine in this study is AC. To Supply AC load, a power converter is used to tie DC bus with the AC one. The converter details are illustrated in Table 3 . The capital, replacement, operational and maintenance costs are assumed as those in [27]. The converter size (P_{conv}) is selected based on load maximum demand (P_{peak}) and inverter efficiency [1].

$$P_{conv}(t) = \frac{P_{peak}(t)}{\eta_{inv}} \tag{10}$$

F. System costs

Objective functions regarding micro-grids design is including the minimization of system costs. Homer select the optimal solution based on NPC and COE which can be calculated as [32].

$$NPC = \frac{TAC}{CRF(i,n)} \tag{11}$$

$$TAC = ACC + ARC + AMC \tag{12}$$

$$CRF = \frac{i(1+i)^n}{(1+i)^n - 1} \tag{13}$$

Where TAC is the total annual cost (\$/year) which is the sum of annual capital cost (ACC), annual replacement cost (ARC) and annual maintenance cost (AMC) for all system components, CRF is the capital recovery factor used to get the recent value of annual value.

It depends on the real interest rate (i) which was taken as 6% and n is the project lifetime of 20 years.

COE is the average cost of kWh of the useful electricity generated by hybrid RE sources. It is calculated in (\$/kWh) by (14) [27].

$$COE = \frac{TAC}{P_l} \tag{14}$$

Where, TAC is the total annual cost and P_l is the total served load over a specific time.

Table 3 Battery and Converter details

Battery		Converter	
Manufactory	Hoppecke-deep cycle battery	Rated power	26 kW
Nominal capacity	1000 Ah	Efficiency	85%
Nominal voltage	2 V	Capital cost	110 \$/kW
Max. depth of discharge DOD	80%	Replacement cost	110 \$/kW
Lifetime throughput	3438 kWh	Lifetime	20 years
Capital cost	50 \$/unit		
Replacement cost	50 \$/unit		
Operational and maintenance	5 \$/unit		
Lifetime throughput	3,438 kWh		

G. Constraints

It is necessary to illustrate program constraints to understand the optimization process. The constraints window inputs are summarized in Table 4.

In most cases, the output power of PV is less than of wind, then the percentage of PV power output is set at value less than the wind power output percentage. Homer calculates the required hourly operating reserve by multiplying these last four factors by the load at this hour and adding to the operating reserve to get reliable results.

Based on the search space for each source, Homer selects the best optimal system combination. With trial and error, the best system is got with inputs search space of 3 - 15 WT units, 190 - 250 PV units, 10 - 30 battery strings and 1 - 4 converter units.

H. Simulation and optimization

For each hour of 8760 hrs. in a year, the system operation is simulated by making energy balance calculations. The hourly electric load is compared to corresponding hourly system energy production by renewable generators. By this comparison, the battery state of charge or discharge can be decided. When the system meets the load for the entire year, Homer estimates the system costs.

After simulating all possible system configurations, a list of feasible system components is displayed and sorted by NPC and COE. The optimal and cost-effective system will be at the top of the list.

IV. RESULTS AND DISCUSSION

Homer is utilized to design the proposed micro-grid. The meteorological data, components' specifications and load profile are defined within Homer. Many cases with different assumptions are assumed to reach the optimal design that minimizes the NPC while keeping constraints including the continuity of the supply.

A. Physical configuration

The configuration of the hybrid PV\WT\battery system is illustrated in Fig. 8. The optimal system is composed of 56.71 kW PV (214 unit × 0.265 kW), 3 WT units, 368 batteries (16 batteries × 23 strings) and 78 kW converter (3 units). The COE is 0.074 \$/kWh.

Performance analysis details are summarized in Table 3. The capacity factors for PV and WT are 26.2 % and 26.8 % respectively. These values are relatively low due to high dumped energy production. The levelized costs for PV and WT are 0.016 and 0.0192 \$/kWh. The battery wear cost is 0.016 \$/kWh, it is the cost of cycling energy through the battery bank. This is approximately 22% of COE.

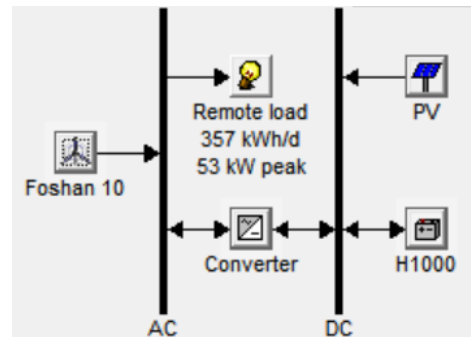


Fig. 8 physical configuration for the hybrid system in Homer

Table 4 Constraints window variables in Homer

Constraints	Setting value	Illustration	
Maximum annual capacity shortage	0%	It is the percentage of the energy difference between the required for load and the actual generated by sources to the total required energy.	
Minimum renewable fraction	100%	As the system under study a PV / Wind system, then it is completely renewable.	
As percent of load	Hourly load percent	10%	It means that the system spare capacity must be kept to cover a 10% sudden increase in hourly load.
	Annual peak load percentage	0%	It is a constant amount of annual operating reserve.
As percent of renewable output	Solar power output	25%	It means that the system must keep supplying the load even if the PV output is decreased by 25%.
	Wind power output	60%	It means that the system must keep supplying the load even if the WT output is decreased by 60%.

The battery expected life is 20 years based on its lifetime throughput. Fig. 9 shows the monthly average production of PV and WT. It can be noted that electric production of WT represents 62% of total production, where PV produces 38%. It is also obvious that PV production is high in summer months due to higher irradiation and temperature.

Batteries wouldn't reach its minimum SOC except in peak hours of load and with poor availability of renewable energy resources. Fig.10 (a) represents the SOC frequencies, it should be pointed out that SOC is almost between 70% to 100% during the year, the frequency is 92.18%. The minimum, maximum and average monthly SOC is shown in Fig.10 (b).

B. Cost analysis

The NPC is 110,314 \$, IC is 89,700 \$, operating cost is 1,797 \$/y and COE is 0.074 \$/kWh. The cost of a battery bank is 39,505 \$ which represent 35.8% of total NPC.

The IC of WT represents 50.67 % of total IC and 42.13% of total NPC. The NPC of PV is 21.7% of total NPC and the converters represent only 0.37% of NPC. Fig. 11 represents the cash flow analysis and costs for system components.

C. Energy balance analysis

The total energy of (341,537 kWh) is generated from PV (38%, 130,085 kWh) and WT (62%, 211,452 kWh). The useful energy is only 43.5% of the total generated energy which covers the total AC load and other losses. The Excess energy counts 56.5% of the total generated energy, this energy had to be dumped as spilled energy [33].

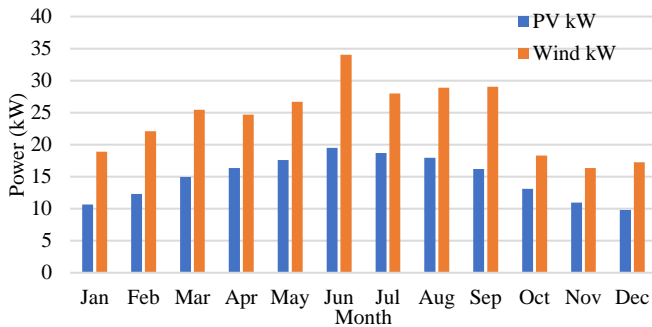


Fig. 9 monthly average electric production of PV and WT

It is necessary to mention that there is a percentage of 1% unmet load although the capacity shortage is set at zero percentage because Homer was set by default to consider any system with fully met load is infeasible.

D. Hourly analysis for sample days

A sample of three consecutive days (27-29 Sept.) is selected to be hourly analyzed as shown in Fig. 12. During 00:00 to 09:00, the load is almost supplied from the batteries, since PV and wind produces very small power. Therefore, SOC is decreased from 97.5 % to 81.2 % during this period. From 09:00 to 18:00, due to the increase in PV and WT output power, batteries charged to a SOC of 99.2 %. PV output power is zero from 19:00 to 5:00, and wind power is less than load demand from 18:00 to 00:00 (the midnight of 28th Sept.). Consequently, the SOC is decreased to 79.8 %. It is clear that the battery is charging at daytime and discharging at night during these three days.

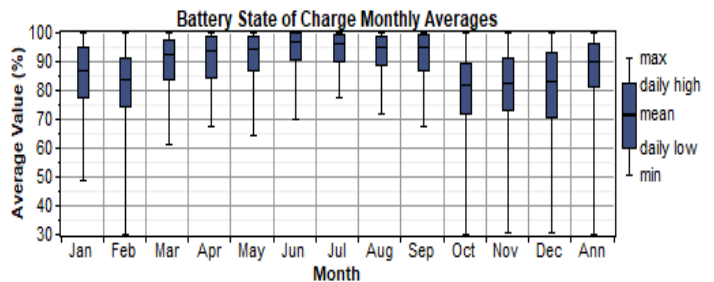
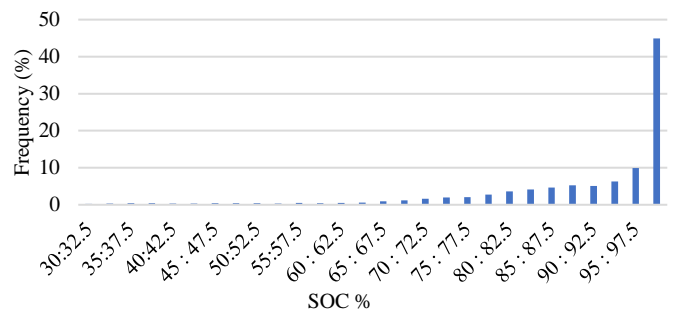


Fig.10 (a)SOC values and frequencies for the simulated year, (b) battery SOC monthly averages

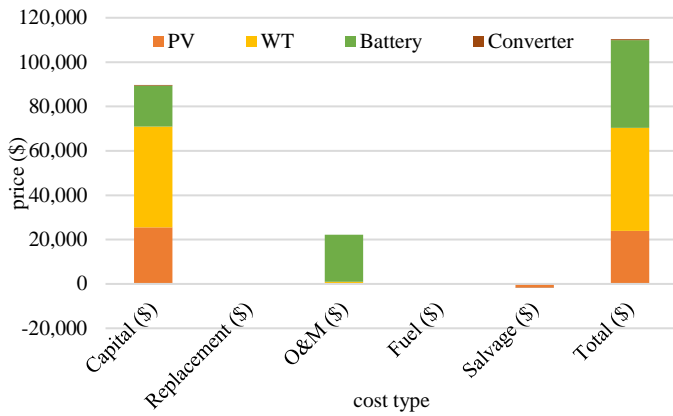


Fig. 11 cash flow and costs for system components for a project life time

In analyzing the hourly data for the whole year, it was found that some-times the surplus power didn't transfer to battery bank although the battery didn't reach its 100% SOC. This is because the battery maximum charging rate and maximum current rate limitations (in this study their values were 1A/Ah, 202A respectively from battery data sheet). Another reason is the battery kinetic model which depend on charging and discharging history of the battery.

It is worth to mention here that although the maximum capacity shortage was set to zero in Homer settings, there was a very small un-met load of 80.6 kWh during the simulated year and its percentage was 0.0256% of the total AC load.

E. Effects of components' sizes on the total NPC

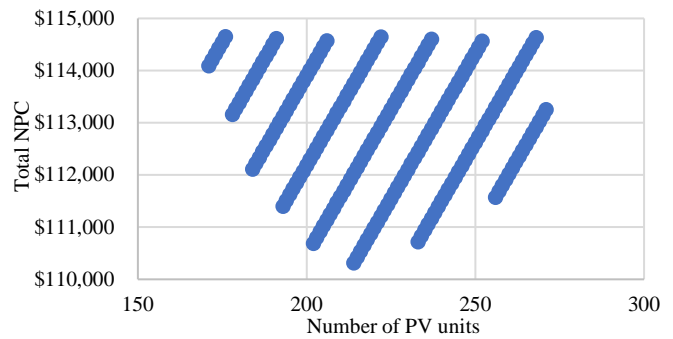
The effect of PV units' variations and battery strings on NPC is illustrated in Fig. 13 (a). The number of WT units is 9 and the converters rating is 78 kW. The lowest NPC is achieved by installing 214 PV units with 23 battery strings. Increasing the number PV units, results in decreasing battery strings. Table 5 shows the variation of PV size, battery units and corresponding NPC and COE with a various number of wind turbines. with increasing WT units, the corresponding PV size and battery units decreased and so as the total NPC, it reaches 110,314 \$ with 9 WTs. Increasing the number of WT units more than 9 results in more COE and NPC. Moreover, the excess energy of the system increases by increasing the number of WT. The conclusion from the aforementioned is that using 9 WT units is considered the most economical solution as shown in Fig. 13 (b).

F. Sensitivity analysis

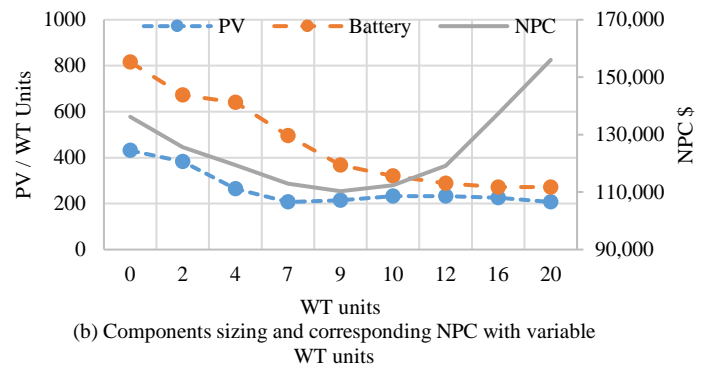
This section introduces the effect of variations of load demand and RE resources on micro-grid design and performance.

1) Variation of load demand

The average load demand is varied in this case study to investigate its effect on components' size. The daily load consumption for the studied case is 357 kWh per day, it is varied here from 250 kWh to 450 kWh per day. Two system configurations are tested, one comprising PV/battery and the other comprising PV/WT/battery. The cropped results are listed in Table 6. Compared to PV/battery system, the PV/WT/battery system has lower COE and NPC, and lower storage capacity. In addition to that, the complementary characteristics between wind and solar energy reduced generation units' sizes, and hence the NPC. Fig. 14 shows the total NPC variations with system type and average daily load for the same zone.



(a) Effect of number of PV and battery strings on NPC



(b) Components sizing and corresponding NPC with variable WT units

Fig. 13 Effect of component sizing variation on NPC (a) with 9 WT units, (b) with variable WT numbers

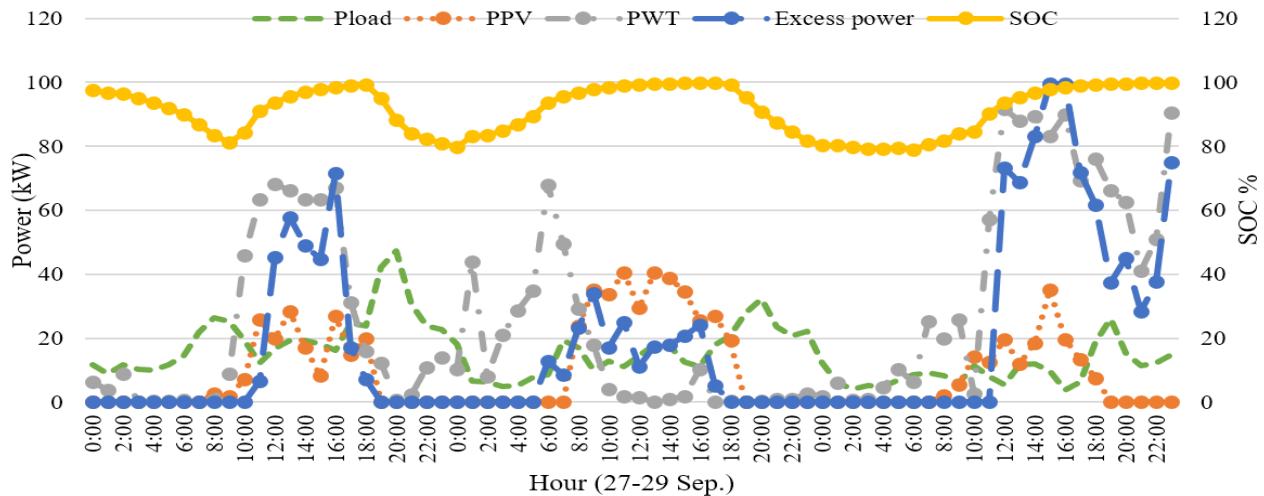


Fig. 12 Hourly power analysis for three consecutive days (27-29 Sep)

Table 5 system configuration under a variable number of WTs

No. of WT	PV size kW	Batteries units	NPC \$	COE \$/kWh	Excess Energy %
0	114.215	816	136,188	0.091	36.9%
2	101.495	672	125,692	0.084	44.4%
4	70.225	640	119,392	0.08	41.0%
7	54.855	496	112,943	0.076	48.4%
9	56.71	368	110,314	0.074	56.5%
10	61.480	320	112,339	0.075	56.9%
12	61.48	288	119,233	0.08	57.1%
16	59.89	272	137,370	0.092	60.7%
20	54.855	272	156,038	0.104	75.7%

2) Renewable resources fluctuations

Due to weather changes and other terrain effects, wind speeds and solar irradiation isn't the same every year. Fig. 15 represents PV and wind production with various wind speeds and solar radiations, this figure is produced by Homer. The NPC illustrated on the profile has lower values with higher values wind speed and solar insolation. With greater insolation and less wind speeds, lower NPC is achieved by using PV/battery system. The same case is found if the cut in speed is less than the assumed value of 3 m/s.

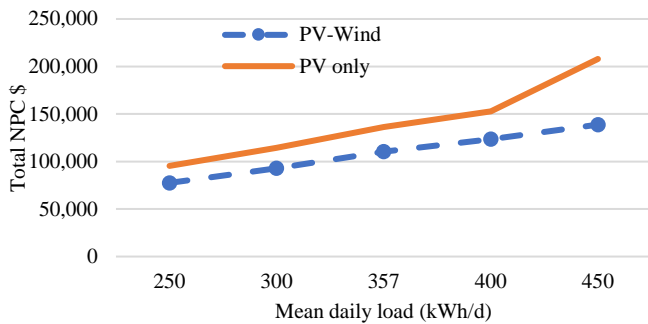


Fig. 14 Total NPC of various mean daily loads

V. CONCLUSION

In this study, an optimal micro-grid is designed in Ras-Shaitan area for an assumed load of 357 kWh/d. The optimal system comprises 56.71kW PV, 9 WTs of 90 kW, 368 batteries, and 78kW converter. The NPC is 110,314 \$ and The COE is 0.074 \$/kWh. PV/WT/battery system is preferable more than PV/battery because of the complementary characteristics of solar and wind energy presented in the study. Results showed that, 38% of the generated energy is supplied from PV and 62% from WT. The dumped generation is 56.5% of the total generated energy. This high percentage is due to the unmatching between load profile and the available power from PV and WT sources. Effect of average load demand and renewable resources fluctuations on system configuration and cost is also presented in this study.

Table 6 Optimal system components size with load variations

Load kWh/d	System type	PV	WT	Batt	Conv.	NPC \$	COE \$/kWh
250	PV\WT\batt	168	6	256	52	77,520	0.074
	PV\batt	289	-	576	52	95,420	0.091
300	PV\WT\batt	182	7	336	52	92,838	0.074
	PV\batt	95.4	-	688	52	114,375	0.091
357	PV\WT\batt	214	9	368	78	110,314	0.074
	PV\batt	431	-	816	78	136,188	0.091
400	PV\WT\batt	240	10	416	78	123,539	0.074
	PV\batt	486	-	912	78	152,643	0.093
450	PV\WT\batt	269	11	480	78	138,816	0.075
	PV\batt	489	-	1424	78	207,942	0.11

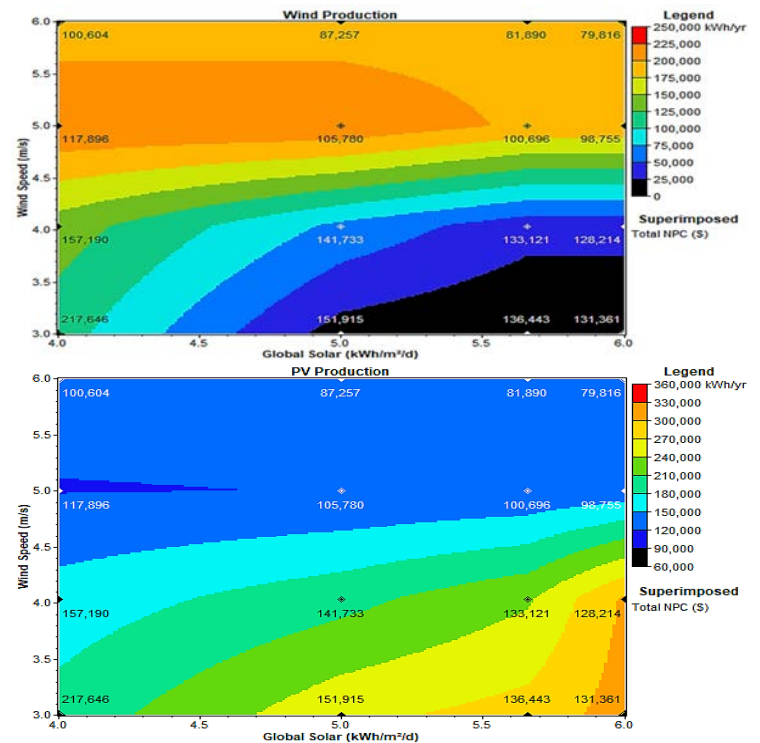


Fig. 15 Rainbow profile of (a) wind production (b) PV production superimposed by NPC

VI. REFERENCES

[1] S. Singh, M. Singh, and S. C. Kaushik, "Feasibility study of an islanded microgrid in rural area consisting of PV, wind, biomass and battery energy storage system," *Energy Conversion and Management*, vol. 128, pp. 178-190, 2016, <https://doi.org/10.1016/j.enconman.2016.09.046>.

[2] L. Qoaider and D. Steinbrecht, "Photovoltaic systems: A cost competitive option to supply energy to off-grid agricultural communities in arid regions," *Applied Energy*, vol. 87, pp. 427-435, 2010, <https://doi.org/10.1016/j.apenergy.2009.06.012>.

[3] T. Tu, G. P. Rajarathnam, and A. M. Vassallo, "Optimization of a stand-alone photovoltaic-wind-diesel-battery system with multi-layered demand scheduling," *Renewable Energy*, vol. 131, pp. 333-347, 2019, <https://doi.org/10.1016/j.renene.2018.07.029>.

- [4] I. Renewables, "analysis and forecasts to 2022–executive summary," Tech rep. International Energy Agency 2017.
- [5] M. Suha Yazici, H. A. Yavasoglu, and M. Eroglu, "A mobile off-grid platform powered with photovoltaic/wind/battery/fuel cell hybrid power systems," *International Journal of Hydrogen Energy*, vol. 38, pp. 11639-11645, 2013, <https://doi.org/10.1016/j.ijhydene.2013.04.025>.
- [6] T. Terlouw, T. AlSkaf, C. Bauer, and W. van Sark, "Multi-objective optimization of energy arbitrage in community energy storage systems using different battery technologies," *Applied Energy*, vol. 239, pp. 356-372, 2019, <https://doi.org/10.1016/j.apenergy.2019.01.227>.
- [7] P. Nikolaidis and A. Poullikkas, "Cost metrics of electrical energy storage technologies in potential power system operations," *Sustainable Energy Technologies and Assessments*, vol. 25, pp. 43-59, 2018, <https://doi.org/10.1016/j.seta.2017.12.001>.
- [8] J. L. Bernal-Agustín and R. Dufo-López, "Simulation and optimization of stand-alone hybrid renewable energy systems," *Renewable and Sustainable Energy Reviews*, vol. 13, pp. 2111-2118, 2009, <https://doi.org/10.1016/j.rser.2009.01.010>.
- [9] A. S. Aziz, M. F. N. Tajuddin, M. R. Adzman, A. Azmi, and M. A. M. Ramli, "Optimization and sensitivity analysis of standalone hybrid energy systems for rural electrification: A case study of Iraq," *Renewable Energy*, vol. 138, pp. 775-792, 2019, <https://doi.org/10.1016/j.renene.2019.02.004>.
- [10] W. Ma, X. Xue, G. Liu, and R. Zhou, "Techno-economic evaluation of a community-based hybrid renewable energy system considering site-specific nature," *Energy Conversion and Management*, vol. 171, pp. 1737-1748, 2018, <https://doi.org/10.1016/j.enconman.2018.06.109>.
- [11] F. Fodhil, A. Hamidat, and O. Nadjemi, "Potential, optimization and sensitivity analysis of photovoltaic-diesel-battery hybrid energy system for rural electrification in Algeria," *Energy*, vol. 169, pp. 613-624, 2019, <https://doi.org/10.1016/j.energy.2018.12.049>.
- [12] M. J. Hadidian Moghaddam, A. Kalam, S. A. Nowdeh, A. Ahmadi, M. Babanezhad, and S. Saha, "Optimal sizing and energy management of stand-alone hybrid photovoltaic/wind system based on hydrogen storage considering LOEE and LOLE reliability indices using flower pollination algorithm," *Renewable Energy*, vol. 135, pp. 1412-1434, 2019, <https://doi.org/10.1016/j.renene.2018.09.078>.
- [13] N. Ghorbani, A. Kasaeian, A. Toopshekan, L. Bahrami, and A. Maghami, "Optimizing a hybrid wind-PV-battery system using GA-PSO and MOPSO for reducing cost and increasing reliability," *Energy*, vol. 154, pp. 581-591, 2018, <https://doi.org/10.1016/j.energy.2017.12.057>.
- [14] A. Giallanza, M. Porretto, G. L. Puma, and G. Marannano, "A sizing approach for stand-alone hybrid photovoltaic-wind-battery systems: A Sicilian case study," *Journal of Cleaner Production*, vol. 199, pp. 817-830, 2018, <https://doi.org/10.1016/j.jclepro.2018.09.223>.
- [15] M. A. M. Ramli, H. R. E. H. Bouchevara, and A. S. Alghamdi, "Optimal sizing of PV/wind/diesel hybrid microgrid system using multi-objective self-adaptive differential evolution algorithm," *Renewable Energy*, vol. 121, pp. 400-411, 2018, <https://doi.org/10.1016/j.renene.2018.01.058>.
- [16] T. Ma, H. Yang, L. Lu, and J. Peng, "Optimal design of an autonomous solar-wind-pumped storage power supply system," *Applied Energy*, vol. 160, pp. 728-736, 2015, <https://doi.org/10.1016/j.apenergy.2014.11.026>.
- [17] R. Dufo-López, J. L. Bernal-Agustín, J. M. Yusta-Loyo, J. A. Domínguez-Navarro, I. J. Ramírez-Rosado, J. Lujano, et al., "Multi-objective optimization minimizing cost and life cycle emissions of stand-alone PV-wind-diesel systems with batteries storage," *Applied Energy*, vol. 88, pp. 4033-4041, 2011, <https://doi.org/10.1016/j.apenergy.2011.04.019>.
- [18] T. Ma, H. Yang, L. Lu, and J. Peng, "Pumped storage-based standalone photovoltaic power generation system: Modeling and techno-economic optimization," *Applied Energy*, vol. 137, pp. 649-659, 2015, <https://doi.org/10.1016/j.apenergy.2014.06.005>.
- [19] D. Connolly, H. Lund, B. V. Mathiesen, and M. Leahy, "A review of computer tools for analysing the integration of renewable energy into various energy systems," *Applied Energy*, vol. 87, pp. 1059-1082, 2010, <https://doi.org/10.1016/j.apenergy.2009.09.026>.
- [20] T. Ma, H. Yang, and L. Lu, "A feasibility study of a stand-alone hybrid solar-wind-battery system for a remote island," *Applied Energy*, vol. 121, pp. 149-158, 2014, <https://doi.org/10.1016/j.apenergy.2014.01.090>.
- [21] H. Z. Al Garni, A. Awasthi, and M. A. M. Ramli, "Optimal design and analysis of grid-connected photovoltaic under different tracking systems using HOMER," *Energy Conversion and Management*, vol. 155, pp. 42-57, 2018, <https://doi.org/10.1016/j.enconman.2017.10.090>.
- [22] R. Sen and S. C. Bhattacharyya, "Off-grid electricity generation with renewable energy technologies in India: An application of HOMER," *Renewable Energy*, vol. 62, pp. 388-398, 2014, <https://doi.org/10.1016/j.renene.2013.07.028>.
- [23] M. Qolipour, A. Mostafaeipour, and O. M. Tousei, "Techno-economic feasibility of a photovoltaic-wind power plant construction for electric and hydrogen production: A case study," *Renewable and Sustainable Energy Reviews*, vol. 78, pp. 113-123, 2017, <https://doi.org/10.1016/j.rser.2017.04.088>.
- [24] A. Haghghat Mamaghani, S. A. Avella Escandon, B. Najafi, A. Shirazi, and F. Rinaldi, "Techno-economic feasibility of photovoltaic, wind, diesel and hybrid electrification systems for off-grid rural electrification in Colombia," *Renewable Energy*, vol. 97, pp. 293-305, 2016, <https://doi.org/10.1016/j.renene.2016.05.086>.
- [25] <https://power.larc.nasa.gov/data-access-viewer/>.
- [26] M. H. Amrollahi and S. M. T. Bathaee, "Techno-economic optimization of hybrid photovoltaic/wind generation together with energy storage system in a stand-alone micro-grid subjected to demand response," *Applied Energy*, vol. 202, pp. 66-77, 2017, <https://doi.org/10.1016/j.apenergy.2017.05.116>.
- [27] T. Ma and M. S. Javed, "Integrated sizing of hybrid PV-wind-battery system for remote island considering the saturation of each renewable energy resource," *Energy Conversion and Management*, vol. 182, pp. 178-190, 2019, <https://doi.org/10.1016/j.enconman.2018.12.059>.
- [28] C. Ghenai and M. Bettayeb, "Modelling and performance analysis of a stand-alone hybrid solar PV/Fuel Cell/Diesel Generator power system for university building," *Energy*, vol. 171, pp. 180-189, 2019, <https://doi.org/10.1016/j.energy.2019.01.019>.
- [29] Z. N. Bako, M. A. Tankari, G. Lefebvre, and A. S. Maiga, "Experiment-Based Methodology of Kinetic Battery Modeling for Energy Storage," *IEEE Transactions on Industry Applications*, vol. 55, pp. 593-599, 2019, <https://doi.org/10.1109/TIA.2018.2866148>.
- [30] A. Malheiro, P. M. Castro, R. M. Lima, and A. Estanqueiro, "Integrated sizing and scheduling of wind/PV/diesel/battery isolated systems," *Renewable Energy*, vol. 83, pp. 646-657, 2015, <https://doi.org/10.1016/j.renene.2015.04.066>.
- [31] J. F. Manwell and J. G. McGowan, "Lead acid battery storage model for hybrid energy systems," *Solar Energy*, vol. 50, pp. 399-405, 1993, [https://doi.org/10.1016/0038-092X\(93\)90060-2](https://doi.org/10.1016/0038-092X(93)90060-2).
- [32] G. Rohani and M. Nour, "Techno-economical analysis of stand-alone hybrid renewable power system for Ras Musherib in United Arab Emirates," *Energy*, vol. 64, pp. 828-841, 2014, <https://doi.org/10.1016/j.energy.2013.10.065>.
- [33] B. Elliston, M. Diesendorf, and I. MacGill, "Simulations of scenarios with 100% renewable electricity in the Australian National Electricity Market," *Energy Policy*, vol. 45, pp. 606-613, 2012, <https://doi.org/10.1016/j.enpol.2012.03.011>.